Molecule Derived Synthesis of Nanocrystalline $YFeO_3$ and Investigations on Its Weak Ferromagnetic Behavior

Sanjay Mathur,*,† Michael Veith,*,‡ Rasa Rapalaviciute,‡ Hao Shen,† Gerardo F. Goya,§ Waldir L. Martins Filho,§ and Thelma S. Berquo§

Leibniz-Institute of New Materials, CVD Division, D-66123 Saarbruecken, Germany, Institute of Inorganic Chemistry, Saarland University, D-66123 Saarbruecken, Germany, and Institute of Physics, University of São Paulo, CP 66318-05389-970 São Paulo, Brazil

Received November 21, 2003. Revised Manuscript Received February 6, 2004

A new Y−Fe alkoxide, $[YFe(OPr^i)_6(Pr^iOH)]_2$, is used in the sol−gel process to obtain the orthoferrite, $YFeO_3$. The Y/Fe stoichiometry (1:1) and Y−O(R)−Fe chemical links in the single molecular precursor kinetically control the formation of metastable $YFeO_3$ which is otherwise difficult to prepare due to the easy formation of the garnet composition, $Y_3Fe_5O_{12}$. TG/DTA analysis showed the crystallization of $YFeO_3$ at 680 °C, which was confirmed by XRD data. The powders obtained were nanocrystalline (TEM) and the only crystalline compound present between 600 and 1300 °C was monophasic $YFeO_3$. The absence of garnet and other iron-containing residual phases observed in previous studies was confirmed by temperature-dependent Mössbauer and magnetization measurements. The magnetization data support a weak ferromagnetic behavior and reveal low- and high-field regimes in M−T and M−H curves, corresponding to magnetocrystalline and antisymmetric-exchange anisotropy, respectively.

Introduction

Chemical synthesis of nanomaterials is based on the transformation of molecular compounds into materials in which the structural units present in the precursor molecule are carried forward to the target solid-state structure.[1−5] This strategy provides the means to grow the solid-state structures from molecular "seeds". For instance, metal alkoxides ($M(OR)_x$) in view of preformed metal−oxygen bonds are efficient precursors to metal oxides (MO_x).[6−10] Although monometal nanocrystalline ceramics (e.g., Al_2O_3, TiO_2, ZrO_2, CeO_2, SnO_2, and Nb_2O_5) have been obtained from molecular chemistry routes, the extension of this approach to multicomponent oxides is rather limited mainly due to the (i) misbelief that the heterometal framework would break down into monometal constituents during the processing steps, and (ii) commercial unavailability of heterometal precursors.[1−10] The use of precursors containing two or more different metallic elements is especially important where the simultaneous growth of different phases and the presence of metastable compounds in the phase-diagram make the phase-selective synthesis a difficult task. For instance, the synthesis of the title compound, $YFeO_3$, is not straightforward because of the preferred formation of $Y_3Fe_5O_{12}$ (YIG) composition in the Y_2O_3−Fe_2O_3 system.[11] Although a number of reports[12−15] are available on $Y_3Fe_5O_{12}$, investigations carried out on the synthesis of the perovskite phase ($YFeO_3$) are limited apparently due to the problematic preparation. Rare earth (RE) orthoferrites ($REFeO_3$) form an important class of weak ferromagnetic materials with interesting magnetic and magnetooptical properties.[16] Yttrium orthoferrite, prepared from the solid-state reactions of the parent oxides or through other physical methods, contains binary (Fe_3O_4) and ternary ($Y_3Fe_5O_{12}$) secondary phases that are undesirable for performing magnetic studies on $YFeO_3$.[17] The weak saturation magnetic moment of the orthoferrite phase is overshadowed by relatively strong magnetic moments of the Fe_3O_4 (magnetite) and $Y_3Fe_5O_{12}$ (garnet) phases. In a preliminary communication, we have reported on the phase-selective synthesis of Gd-

* Address correspondence to S.M. Tel: 0049-681-9300-338. Fax: 0049-681-9300-279. E-mail: smathur@inm-gmbh.de.
† Leibniz-Institute of New Materials.
‡ Saarland University.
§ University of São Paulo.

(1) Veith, M. *Dalton Trans.* **2002**, 2405.
(2) Mathur, S. In *Chemical Physics of Thin Film Deposition Processes for Micro- and Nano-Technologies*; NATO ASI, Kluwer Academic Publishers: Dordrecht, The Netherlands, 2002; p 91.
(3) Cowley, A. H.; Jones, R. A. *Angew. Chem.* **1989**, *101*, 1235.
(4) Trindade, T.; O'Brien, P.; Pickett, N. L. *Chem. Mater.* **2000**, *13*, 3843.
(5) Gillan, E. G.; Barron, A. R. *Chem. Mater.* **1997**, *9*, 3037.
(6) Bradley, D. C. *Chem. Rev.* **1989**, *89*, 1317.
(7) Hubert-Pfalzgraf, L. G. *Polyhedron* **1994**, *8*, 1181.
(8) Mehrotra, R. C.; Singh, A. *Chem. Soc. Rev.* **1994**, 215.
(9) Veith, M.; Mathur, S.; Mathur, C. *Polyhedron* **1998**, *17*, 1005.
(10) Chandler, C. D.; Roger, C.; Hampden-Smith, M.-J. *Chem. Rev.* **1993**, *93*, 1205.
(11) Buscaglia, V.; Caracciolo, F.; Bottino, C.; Leoni, M.; Nanni, P. *Acta Mater.* **1997**, *45*, 1213.
(12) Ristic, M.; Nowik, I.; Popovic S.; Felner, I.; Music, S. *Mater. Lett.* **2003**, *57*, 2584.
(13) Taketomi, S.; Dai, Z. R.; Ohuchi, F. S. *J. Magn. Magn. Mater.* **2000**, *217*, 5.
(14) Ahn, Y. S.; Ahn, M. H.; Kim, C. O. *J. Mater. Sci.* **1996**, *31*, 4233.
(15) Sankarnarayanan V. K.; Gajbhiye, N. S. *J. Am. Ceram. Soc.* **1990**, *73*, 1301.
(16) (a) Didosyan, Y. S.; Hauser, H.; Wolfmayer, H.; Nicolics, J.; Fulmek, P. *Sens. Actuators A* **2003**, *106*, 168. (b) Didosyan, Y. S.; Hauser, H.; Toriser, W. *Int. J. Appl. Electrom.* **2001**, *13*, 277.
(17) Schmool, D. S.; Keller, N.; Guyot, M.; Krishnan, R.; Tessier, M. *J. Magn Magn. Mater.* **1999**, *195* (2), 291.

10.1021/cm0311729 CCC: $27.50
Published on Web 04/24/2004

Scheme 1. Representation of $YFeO_3$ unit cell

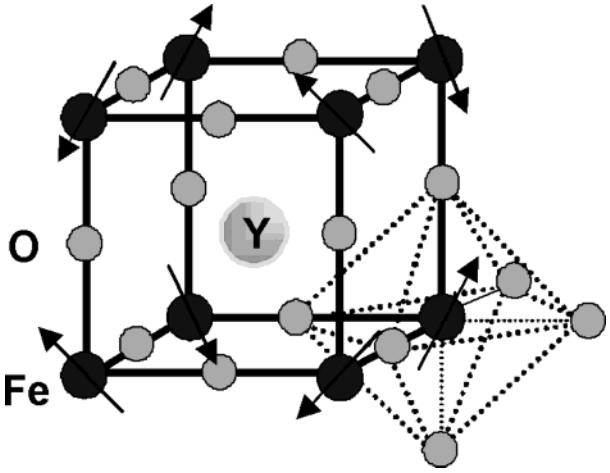

FeO_3 from a single molecular precursor.[18] We describe here the sol−gel processing of a Y−Fe mixed-metal alkoxide, $[YFe(OPr^i)_6(Pr^iOH)]_2$ that is an effective molecular scaffold to synthesize $YFeO_3$ nanoparticles with a precise chemical composition and particle size control. The existence of −Y−O(R)−Fe− linkages in the precursor and an appropriate Y/Fe ratio enforces the formation of $YFeO_3$ with a precise stoichiometry control and prevents any element segregation generally observed in conventional methods.[1,2]

The orthoferrite $YFeO_3$ crystallizes in a distorted perovskite structure with an orthorhombic unit cell.[19] The distortion from the ideal perovskite is mainly in the position of the yttrium ions, whereas the Fe^{3+} ions are present in an essentially octahedral environment. The structure can be visualized as a three-dimensional network of strings of FeO_6 octahedra. One of the anions (O^{2-}) forms the common apex of the two adjacent octahedra and provides the super-exchange bond (Fe−O−Fe) between two iron ions (Scheme 1). Thus each iron ion is coupled by super-exchange to six nearest (iron) neighbors. Because the alignment of Fe moments is not strictly antiparallel but slightly canted, a small net magnetization results, giving rise to a weak ferromagnetic (WFM) behavior. The WFM component is produced by an antisymmetric exchange (Dzyaloshinski−Moriya, DM) interaction[20] of the form $-\mathbf{D}\cdot(\mathbf{M_1} \times \mathbf{M_2})$ ($\mathbf{M_1}$ and $\mathbf{M_2}$ being the sublattice magnetizations of two neighboring Fe ions) that tends to align the $\mathbf{D}$, $\mathbf{M_1}$, and $\mathbf{M_2}$ vectors perpendicular to each other to minimize the coupling energy. This distinctive magnetic structure is reflected in the coexistence of small and high anisotropy fields associated with magnetocrystalline and DM interactions, respectively. The remarkable properties of orthoferrites such as high domain-wall velocity[21] and the existence of Bloch lines,[22] have significance for applications in magnetic field sensors and magnetooptical data storage devices.[16,23] However, the difficulties

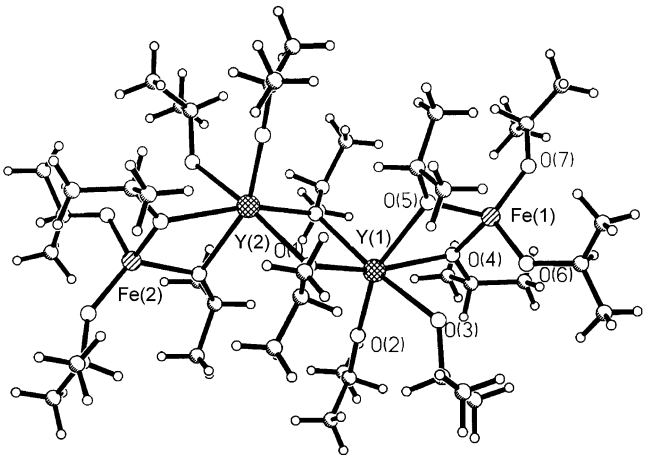

Figure 1. Molecular structure of $[YFe(O^iPr)_6(Pr^iOH)]_2$.

encountered in synthesizing single-phase rare-earth orthoferrites is probably responsible for their less-explored technological potential when compared to that of garnet materials.[16,18] High density, single-phase materials with a controlled microstructure are required for optimal properties. The aim of this work was to synthesize monophasic $YFeO_3$ using "soft chemistry" methods and to investigate the weak ferromagnetic behavior in resulting orthoferrite nanoparticles.

Experimental Section

Chemicals. The syntheses of metal alkoxides[24] and amides[25] were performed in a modified Schlenk type vacuum assembly, taking stringent precautions against atmospheric moisture. Solvents were purified by standard methods and stored over appropriate desiccating agents. Yttrium (III) chloride (Aldrich) was dried in vacuum (110 °C/10^{-2} Torr) and analyzed for chlorine contents before use. The synthesis of yttrium tris(silylamide), $[Y\{N(SiMe_3)_2\}_3]$, and its reaction with excess *tert*-butyl alcohol to obtain $[Y_3(OBu^t)_9(Bu^tOH)_2]$ are described elsewhere.[26] $[Fe_2(OBu^t)_6]$ was synthesized by a salt elimination reaction between $FeCl_3$ and three equiv of $NaOBu^t$ in a mixture of tetrahydrofuran and toluene, followed by sublimation in vacuum (80 °C/10^{-2} Torr).[27]

Precursor and Nanoparticle Synthesis. Heterometal alkoxide, $[YFe(OPr^i)_6(Pr^iOH)]_2$ (Figure 1) was prepared by a ligand exchange reaction (eq 1) in which an equimolar reaction of yttrium and iron *tert*-butoxide was treated with an excess of isopropyl alcohol. The reaction mixture was refluxed (∼4 h) and the amount of the solvent was reduced in a vacuum to obtain a colorless solid. Upon recrystallization from a toluene−isopropyl alcohol mixture, kept at −5 °C overnight, rectangular bars of $[YFe(OPr^i)_6(Pr^iOH)]_2$ (> 70%) were obtained. The chemical analysis (Y, Fe, C, and H) of the crystalline material corresponded to the proposed formulation and a Y/Fe ratio of 1:1, which was confirmed by a single-crystal X-ray diffraction analysis (see below).

$$2[Y_3(OBu^t)_9(Bu^tOH)_2] + 3\,[Fe_2(OBu^t)_6] \xrightarrow{Pr^iOH(excess)} 3\,[YFe(OPr^i)_6(Pr^iOH)]_2 + 40\,Bu^tOH \quad \text{... (1)}$$

The sol−gel processing of the heterometal precursor proceeds via partial hydrolysis (activation) and condensation

(18) Mathur, S.; Shen, H.; Lecerf, N.; Kjekshus, A.; Fjellvåg, H.; Goya, G. F. *Adv. Mater.* **2002**, *14* (19), 1405.
(19) (a) Geller, S.; Wood, E. A. *Acta Crystallogr.* **1956**, *9*, 563. (b) Geller, S. *J. Chem. Phys.* **1956**, *24*, 1236.
(20) Dzyaloshinsky, I. E. *J. Phys. Chem. Solids* **1958**, *4*, 241.
(21) Didosyan, Y. S.; Hauser, H. *Phys. Lett. A* **1998**, *238*, 395.
(22) Didosyan, Y. S.; Barash, V. Y.; Bovarin, N. A.; Hauser, H.,; Fulmek, P. *Sens. Actuators A* **1997**, *59*, 56.
(23) Ripka, P.; Vértesy, G. *J. Magn. Magn. Mater.* **2000**, *215*, 795.
(24) Bradley, D. C.; Mehrotra, R. C.; Gaur, D. P. *Metal Alkoxides*; Academic Press: London, 1978.
(25) Lappert, M. F.; Power, P. P.; Sanger, A. R.; Srivastava, R. *Metal and Metalloid Amides*; Ellis Horwood-Wiley: New York, 1980.
(26) Veith, M.; Mathur, S.; Kareiva, A.; Jilavi, M.; Zimmer, M.; Huch, V. *J. Mater. Chem.* **1999**, *9*, 3069.
(27) Mathur, S.; Veith, M.; Sivakov, V.; Shen, H.; Huch, V.; Hartmann, U.; Gao, H. B. *Chem. Vap. Deposition* **2002**, *8* (6), 277.

reactions. Briefly, $[YFe(OPr^i)_6(Pr^iOH)]_2$ (1.931 g, 1.726 mmol) was dissolved in hot (60 °C) isopropyl alcohol and carefully hydrolyzed by adding 3−4 mol of water in isopropyl alcohol. The resulting solution was stirred for 12 h to obtain a homogeneous sol. The slow evaporation (50 °C) of solvent produced a yellowish transparent gel, which was oven-dried (120 °C, 6 h) to obtain a fluffy powder (xerogel) that was shown to be amorphous by powder X-ray diffraction. The xerogel was ground, heated in a laboratory furnace at 300 °C to burn out the organic residues, and calcined at higher temperature (600−1400 °C) to obtain nanocrystalline $YFeO_3$ with different average particle sizes.

Characterization. X-ray crystallography on the single-crystal specimen of $[YFe(OPr^i)_6(Pr^iOH)]_2$ was performed on a Siemens Stoe AED 2 diffractometer fitted with graphite monochromatic Mo Kα X-ray radiation (λ = 0.71073 Å). A suitable crystal was sealed in a glass capillary under dry nitrogen atmosphere and was mounted on the goniometer head for the data collection. Data were collected at room temperature using the $\omega-\theta$ scan technique. The crystal structure was solved and refined using the SHELXS package for crystal structure solution and refinement.[28] For studying the decomposition pathway, the xerogel was placed in a TGA/DTA crucible and heated to 1050 °C, with a ramp of 5 °C/min. The chemical composition of powder compacts was determined by electron spectroscopy for chemical analysis (ESCA) performed on a Surface Science Instrument, M-Probe, operating with an Al Kα radiation and a total instrumental resolution (fwhm, full width at half-maximum) of ca. 0.8 eV. Particle morphology and elemental distribution in xerogel and calcined powders were recorded using a scanning electron microscope JSM-6400F (JEOL) coupled with an energy dispersive X-ray (EDX) facility. The FTIR spectra were recorded in a KBr matrix on a Biorad-165 Fourier transform spectrometer. Powder X-ray diffraction data were collected with a STOE diffractometer (STADIP) operating with a Cu Kα radiation. XRD data were used to calculate the average sizes of the orthoferrite nanoparticles from the magnitude of the half width of three major peaks, using Scherer's formula. TEM analyses were performed by drawing an amorphous carbon-coated copper grid through sonicated dispersions (Pr^iOH) of the samples calcined at different temperatures. Magnetic measurements on powdery samples, dispersed in epoxy resin, were accomplished using a commercial SQUID magnetometer at temperatures of 2 K ≤ T ≤ 400 K and applied fields up to 70 kOe. Variable-temperature (4.2−295 K) Mössbauer spectra were recorded in transmission geometry, using a $^{57}Co/Rh$ source in the constant acceleration mode. All spectra were fitted using Lorentz line shapes with isomer shifts referred to α-Fe at room temperature.

Results and Discussion

Thermodynamically labile phases cannot be selectively prepared by traditional processing routes due to rather harsh reaction conditions that are driven by equilibrium thermodynamics. In this context, the chemical reactions based on controlled interaction of atoms or molecules in vapor or liquid phase are viable alternatives to obtain metastable compounds as nanostructured films or particles.[1−5,29,30] However, a straightforward synthesis is not guaranteed by all chemical approaches, and the processing of mixed-oxide ceramics by conventional wet-chemical techniques does not always lead to a stoichiometric compound. The major problems faced are component segregation, mixed phases, or nonideal stoichiometry in the final ceramic material caused by intrinsic differences in the chemical properties of the reacting species. In binary phases, the combination of both phase-forming cations in a single molecule offers a control over the reaction kinetics and facilitates selective synthesis of metastable phase such as orthoferrites. Therefore, precursors containing the phase-forming elements in a single molecule are promising starting materials for solid-state materials; for example, the heterometal alkoxide, $[YFe(OPr^i)_6(Pr^iOH)]_2$, as precursor to $YFeO_3$.

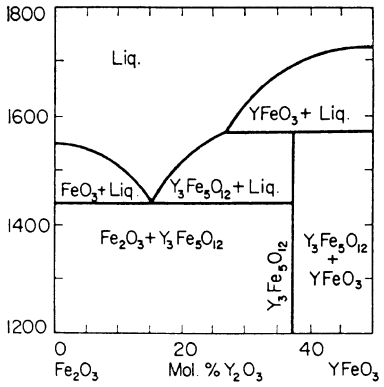

Figure 2. $Y_2O_3-Fe_2O_3$ binary phase diagram.

Among the two ternary oxides present in the $Y_2O_3-Fe_2O_3$ system, namely $YFeO_3$ and $Y_3Fe_5O_{12}$, the formation of later compound is favored, as shown by growth kinetics studies.[11]

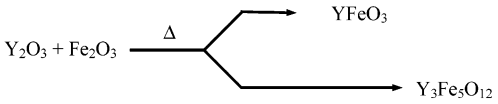

The phase diagram supports the observed phase separation and an easy formation of the garnet composition (Figure 2),[31] when the Y-Fe compounds are formed by the solid-state reaction of iron and yttrium oxides. Although wet-chemical methods such as coprecipitation or polymeric precursor processing are suitable for the synthesis of several bimetallic oxides, their application to orthoferrites is not advantageous. In the case of yttrium iron garnet, the coprecipitaion of Y and Fe hydroxides, or complexation of Y^{3+} and Fe^{3+} ions by a polymeric agent, significantly lowers the processing temperature because the diffusion paths are reduced.[14] Nevertheless, the reaction still occurs through bulk diffusion and is thus governed by growth kinetics. However, if the interacting Y^{3+} and Fe^{3+} ions are chemically bonded (e.g., Y−O(R)−Fe), there is no need of a diffusion for the phase formation. This strategy implicates a control over the chemical composition during the phase evolution provided the heterometal bridges remain intact under the processing conditions.

The single-crystal diffraction analysis (Figure 1) of the compound $[YFe(OPr^i)_6(Pr^iOH)]_2$,[32] shows −Y−O(Pr^i)−

(28) (a) Sheldrick, G. M. *SHELXS-86, Program of Crystal Structure Determination*; University of Göttingen, Göttingen, Germany, 1986. (b) Sheldrick, G. M. *SHELXS-97, Program of Crystal Structure Determination*; University of Göttingen, Göttingen, Germany, 1997.

(29) Veith, M.; Mathur, S.; Lecerf, N.; Huch, V.; Decker, T.; Beck, H. P.; Eiser, W.; Haberkorn, R. *J. Sol-Gel Sci. Technol.* **2000**, *17*, 145.

(30) Rao,C. N. R. *Chemical Approaches to the Synthesis of Inorganic Materials*; John Wiley: New York, 1994.

(31) Nielsen, J. W.; Dearborn, E. F. *Phys. Chem. Solids* **1958**, *5*, 203.

(32) $C_{42}H_{100}Fe_2Y_2O_{14}$; crystal system, triclinic; space group, $P\bar{1}$; a = 11.046 Å, b = 12.203 Å, c = 13.193 Å; α = 80.26°, β = 67.40°, γ = 71.49°; V = 1559.3 Å^3; Z = 2; reflections collected, 4448; independent reflections, 4186; R = 0.0273, wR [$I > 4\sigma I$] = 0.0293.

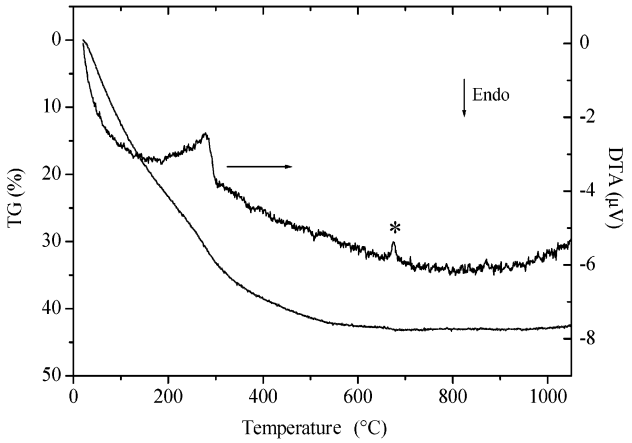

Figure 3. TG/DTA profiles of Y−O−Fe xerogel.

Fe− linkages and a Y/Fe ratio of 1:1, which qualifies it as a *single molecular source* to $YFeO_3$. The molecule is a centrosymmetric dimer with a one-dimensional arrangement of Y and Fe ions bridged through isopropoxy groups. The coordination polyhedra of Fe and Y atoms can be described as slightly distorted tetrahedra and octahedra, respectively, that share edges in the crystal structure. The coordination sphere of Y(III) atoms contains a coordinated neutral isopropyl alcohol molecule, which completes the octahedral configuration. The sol−gel processing of $[YFe(OPr^i)_6(Pr^iOH)]_2$ and the phase characterization in the resulting xerogel and calcined powder shows the formation of $YFeO_3$ ceramic at the molecular level (eq 2).

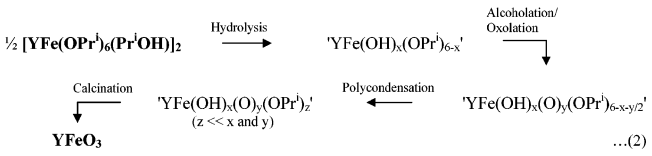

...(2)

To decipher the low-temperature decomposition steps, the calcination behavior was studied up to 1050 °C using TG−DTA analysis. The DTA curve (Figure 3) exhibits a broad peak in the temperature range 220−350 °C, possibly associated with the elimination of bound water and organics present in the dried gel. The dehydration and decomposition processes are evident in the TG curve as supported by a continuous decrease in the sample weight (Figure 3). The exothermic peak at ca. 680 °C does not correspond to a major weight loss in the TG curve and suggests the crystallization of the yttrium orthoferrite phase that is supported by the powder XRD data. A minor weight loss observed in the DTA curve may be due to dehydroxylation of the residual hydroxy groups that occurs at the oxide crystallization temperature.[29] These observations are corroborated by the FTIR data of the xerogel calcined at different temperatures (Figure 4). The IR spectra of the powder calcined at 400 and 600 °C show peaks in the range 1300−1600 cm^{-1} that are characteristic for metal-bound isopropoxy groups.[24,26,33] As found in the TG−DTA analysis, the powder heat-treated above 600 °C is free from organic groups. The IR spectra of the powders heat-treated at higher temperatures show the characteristic spectral

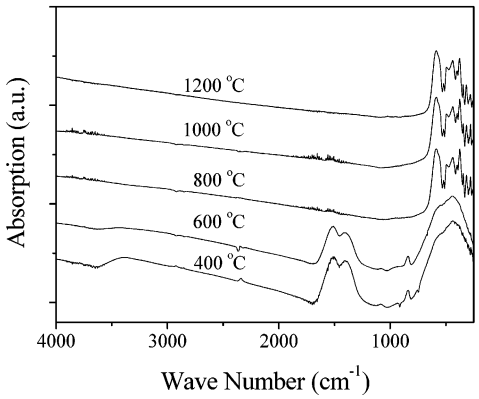

Figure 4. FTIR spectra of xerogels calcined at 400, 600, 800, 1000, and 1200 °C.

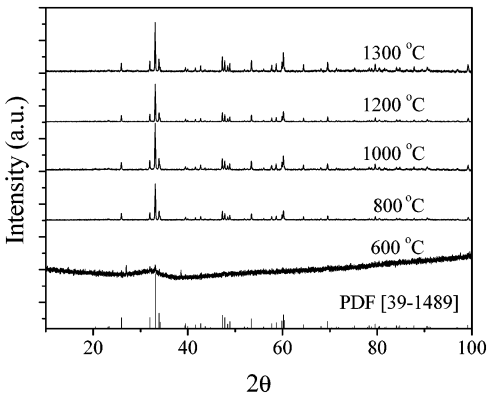

Figure 5. Room-temperature X-ray diffractograms of $YFeO_3$ calcined at 600, 800, 1000, 1200, and 1300 °C. Solid lines denote orthorhombic $YFeO_3$, PDF [39-1489].

patterns for orthoferrite phase.[34] The Y−O and Fe−O stretching frequencies are observed in the typical range reported for Y_2O_3−Fe_2O_3 systems.[12,25]

Figure 5 shows the XRD patterns of the amorphous xerogel and powders calcined at 600, 800, 1000, 1200, and 1300 °C. The onset of crystallization process in the sample calcined at 600 °C is noticeable in the incipient peaks, although the low intensity indicates a poorly crystalline state of the sample. A single-phase $YFeO_3$ is already formed at 800 °C. The evolution of the diffractograms with increasing calcination temperatures shows a steady decrease of line width due to increasing particle sizes. No other phases are observed up to 1300 °C which is in contrast to other reports where garnet and/or iron oxide phases are invariably formed in the processing of orthoferrite composition.[35,36] In agreement with XRD data, TEM micrographs (Figure 6a−d) of sample calcined at different temperatures show nanometric grains with a gradual increase in the average particle size upon increasing calcination temperatures. The high-resolution image (Figure 6e) of a sample heat-treated at 800 °C shows highly crystalline grains with well-defined lattice planes.

The elemental composition and the oxidation-state of the cations were determined by the XPS analysis of a $YFeO_3$ powder compact. Figure 7 shows the overview

(33) Meyer, F.; Hempelmann, R.; Mathur, S.; Veith, M. *J. Mater. Chem.* **1999**, *9*, 1755.

(34) Mathur, S.; Veith, M.; Rapalaviciute, R. (unpublished results).

(35) Schmool, D. S.; Keller, N.; Guyot, M.; Krishnan, R.; Tessier, M. *J. Appl. Phys.* **1999**, *86* (10), 5712.

(36) Cao, X.; Kim, C.-S.; Yoo, H.-I. *J. Am. Ceram. Soc.* **2001**, *84*, 1265.

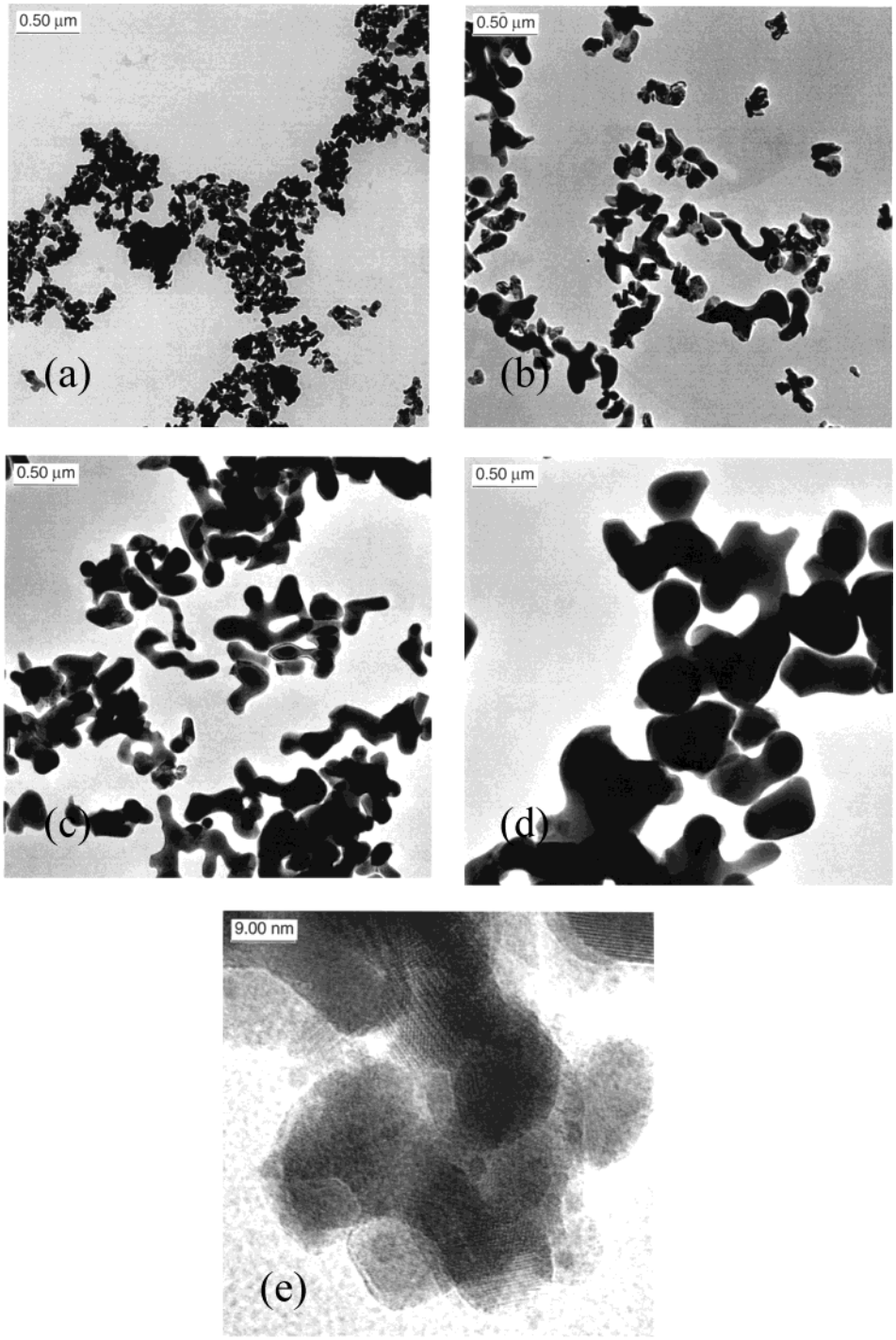

Figure 6. TEM images (a−d) of $YFeO_3$ samples calcined at 600, 800, 1000 and 1200 °C, respectively. (e) HREM image of $YFeO_3$ sample (800 °C) showing highly crystalline grains and individual lattice planes.

XPS spectrum of $YFeO_3$ powder, calcined at 800 °C, which reveals Y and Fe present in 1:1 ratio. Although trivalent oxidation state is commonly observed for yttrium compounds, iron cations are prone to redox reactions and relatively more stable in subvalent states. As a result, a partial reduction of Fe^{3+} to Fe^{2+} through a deficiency of oxygen and/or the reducing action of the liberated organic byproducts is not improbable in iron containing systems.[33] It should be noted that the formation of magnetite ($Fe^{2+}Fe_2^{3+}O_4$) is observed during the synthesis of $YFeO_3$ from Y(III) and Fe(III) precursors.[17,35,36] A comparison of the Fe 2p XPS spectrum (Inset, Figure 7) of the $YFeO_3$ sample with those of the standard iron oxides, Fe_2O_3, and FeO single crystals ruled out the presence of Fe(II) species.[37] This was further supported by the Mössbauer data of the samples (vide infra). The Fe 2p core level spectra are split due to the spin−orbit coupling into $2p_{3/2}$ and $2p_{1/2}$ components. The Fe $2p_{3/2}$ peak observed in $YFeO_3$ matches well with the Fe^{3+} binding energy of Fe_2O_3 sample. In addition, the Fe 2p spectrum of Fe_2O_3 shows a satellite at 718.5 eV, which is a diagnostic feature for the Fe^{3+} species and is also present in the $YFeO_3$ sample. The

(37) Fujii, T.; de Groot, F. M. F.; Sawatzky, G. A.; Voogt, F. C.; Hibma, T.; Okada, K. *Phys. Rev. B* **1999**, *59*, 3195.

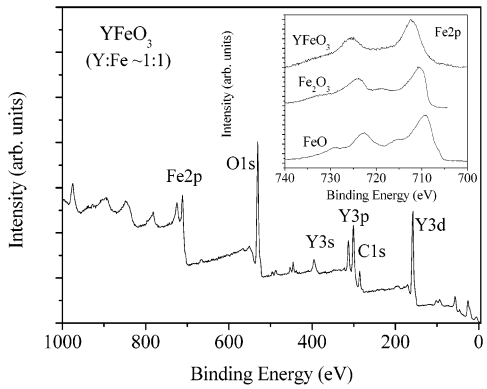

Figure 7. Overview XPS spectrum of $YFeO_3$ powder calcined at 800 °C. The Fe 2p XPS spectra of $YFeO_3$, Fe_2O_3, and FeO are shown in the inset.

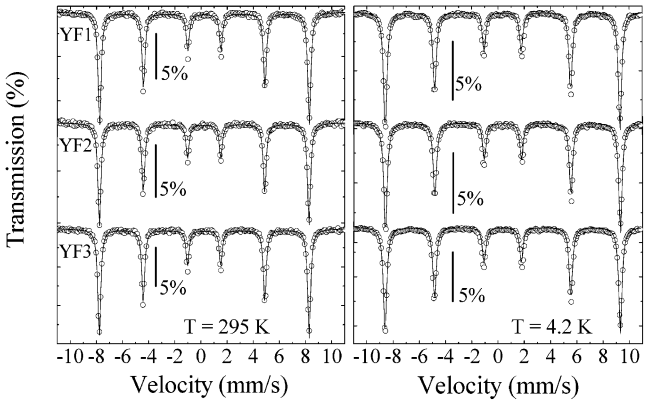

Figure 8. (a) Room- and (b) low-temperature (4.2 K) Mössbauer spectra of **YF1**, **YF2**, and **YF3** samples calcined at 800, 1000, and 1200 °C.

Table 1. Hyperfine Parameters Obtained from the Mössbauer Spectra Recorded at 4.2 and 295 K with Hyperfine Field (B), Isomer Shift (IS), Quadrupole Splitting (QS), and Linewidth (Γ) Values[a]

T (K)	T_{ann} (°C)	B (Tesla)	IS (mm/s)	QS (mm/s)	Γ (mm/s)
4.2	800	55.3(1)	0.461(3)	0.002(6)	0.33(1)
	1000	55.3(1)	0.460(3)	0.002(6)	0.34(1)
	1200	55.3(1)	0.462(3)	0.004(6)	0.34(1)
295	800	49.9(1)	0.358(2)	0.008(2)	0.27(1)
	1000	49.8(1)	0.356(3)	0.006(2)	0.27(1)
	1200	49.9(1)	0.357(3)	0.008(2)	0.27(1)

[a] Samples labeled **YF1**, **YF2**, and **YF3** were calcined at 800, 1000 and 1200 °C, respectively.

trivalent oxidation state of yttrium in $YFeO_3$ sample was confirmed by comparing the binding energy of Y 3p peak with that of yttrium aluminum garnet, $Y_3Al_5O_{12}$, which showed no fine differences between the two systems.[26,38]

Room-temperature Mössbauer spectra (Figure 8a) of samples calcined at 800 (**YF1**), 1000 (**YF2**), and 1200 °C (**YF3**) show a single magnetic sextet for Fe^{3+} ions in $YFeO_3$ with hyperfine parameters (Table 1) consistent with previously reported values.[39,40] The remarkably small line width (Γ ≈ 0.27 mm/s) of the three spectra

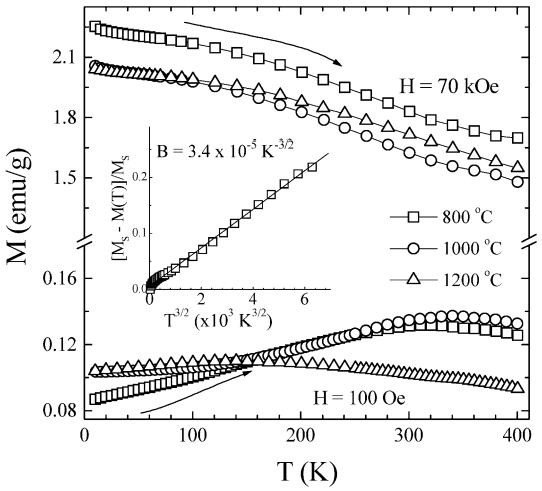

Figure 9. Temperature-dependent magnetization curves of **YF1**, **YF2**, and **YF3** samples at applied magnetic fields of 100 Oe (lower curves) and 70 kOe (upper curves). Inset: Normalized magnetization vs $T^{3/2}$, showing the linear dependence.

exhibits excellent crystallinity of the present samples. In agreement with the XRD and XPS data discussed above, the present samples show no evidence of additional Mössbauer lines from secondary Fe-containing phases, within experimental accuracy (~2% of the spectral area). As displayed in Figure 8, the expected increment of hyperfine field values was observed on lowering the temperature (from 49.9 to 55.3 Tesla at 294 and 4.2 K, respectively). The low-temperature value is slightly larger than that in previous reports,[40,41] which might be attributed to a high local atomic order in the samples that favors the Fe−O−Fe superexchange interactions.

The temperature-dependent magnetization curves of **YF1**, **YF2**, and **YF3** samples at applied field H = 100 Oe and 70 kOe are shown in Figure 9. For **YF1** and **YF2**, a broad maximum can be discerned at T ≈ 350 K, whereas the maximum, centered around 100 K, is less pronounced in **YF3**. The different behavior observed at low fields may likely be related to the small anisotropy of the WFM component, which in turn is attributed to the small magnetocrystalline anisotropy field $H_B \approx 300$ Oe, typical for $YFeO_3$.[42] Therefore, the observed differences should not appear if the external fields suffice to overcome the anisotropy ($H_{app} > H_B$). Accordingly, at higher applied fields ($H_{app} \geq 3$ kOe), all the three samples show very similar behavior, and moreover the M(T) is found to be proportional to $T^{3/2}$, as expected for saturating magnetic moments at low temperatures. The high-field M(T) curves conform with the Bloch law (eq 3) as shown in the inset of Figure 9.[43]

$$M_S(T) = M_S(0)(1 - BT^{3/2}) \ldots \quad (3)$$

where $M_S(0)$ is the saturation magnetization at zero temperature and the value of B ($2.9-3.4 \times 10^{-5}$ $K^{-3/2}$) depends on the samples. The B values in **YF1**, **YF2**, and **YF3** are larger than those found for simple metals such as α-Fe (3.4×10^{-6} $K^{-3/2}$) probably due to the combined

(38) Crist, B. V. *Handbook of Monochromatic XPS Spectra*; Wiley Europe: Chichester, U.K., 2000.
(39) Eibschutz, M.; Gorodetsky, G.; Shtrikman, S.; Treves, D. *J. Appl. Phys.* **1964**, *35*, 1071.
(40) Eibschutz, M.; Shtrikman, S.; Treves, D. *Phys. Rev.* **1967**, *156*, 562.
(41) Durbin, G. W.; Johnson, C. E.; Thomas, M. F. *J. Phys. C: Solid State Phys.* **1975**, *8*, 3051.
(42) Treves, D. *Phys. Rev.* **1962**, *125*, 1843.
(43) Bloch, F. *Z. Phys.* **1930**, *61*, 206.

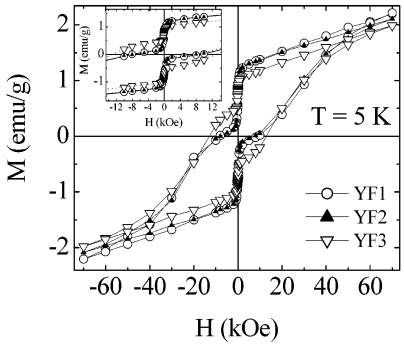

Figure 10. Hysteresis loops recorded at 5 K for **YF1** (open circles), **YF2** (solid triangles), and **YF3** (open triangles), after cooling the samples in zero external field. Inset: Magnification of the low field region.

effect of exchange and DM interactions. A linear relation between ΔM_S vs $T^{3/2}$ is observed along the whole experimental temperature range (5 K $\leq$ T $\leq$ 330 K), suggesting the existence of spin-wave excitations (Inset, Figure 9). Theoretical calculations[44] have predicted a relation $\Delta M \approx T^{\alpha}$ ($^3/_2 < \alpha < 3$) for ferromagnetic clusters, although experimental evidence of Bloch behavior ($\alpha = {}^3/_2$) has been reported for many systems such as α-Fe particles in SiO_2 matrix[45] and γ-Fe_2O_3 particles.[46,47] The values of prefactor B obtained from our $YFeO_3$ samples are very close to the values ($2.8-3.3 \times 10^{-5}$ $K^{-3/2}$) observed from other nanostructured oxides such as Fe_3O_4 and γ-Fe_2O_3 particles.[46,48]

It is well-known that the $YFeO_3$ magnetic structure can be described as composed by two Fe magnetic sublattices that display weak ferromagnetic (WFM) ordering. The magnetic interactions in $YFeO_3$ according to Treves[49] can be described by the expression

$$E = \lambda \mathbf{M_1}\cdot\mathbf{M_2} - \mathbf{H}\cdot(\mathbf{M_1} + \mathbf{M_2}) - \mathbf{D}\cdot(\mathbf{M_1} \times \mathbf{M_2}) - (K_B/M_0^2)(M_{1x}^2 + M_{2x}^2) \quad (4)$$

where $\mathbf{M_0} = |\mathbf{M_1}| = |\mathbf{M_2}|$, $\mathbf{M_1}$ and $\mathbf{M_2}$ being each Fe-sublattice magnetization. The first and second terms are related to the isotropic exchange and external magnetic field interactions, respectively. The third term represents the DM antisymmetric interaction, which is a minimum when each sublattice magnetization $\mathbf{M_1}$ and $\mathbf{M_2}$ and the **D** vectors are mutually perpendicular, and the last term comes from magnetocrystalline anisotropy effects. For solving eq 4 in terms of interaction fields, one defines the exchange field $H_E = \lambda M_0$, the DM anisotropy field $H_D = D M_0$, and the magnetocrystalline anisotropy field $H_B = 2K_B/M_0$. Assuming further that the WFM component is in the *z*-direction, we have $H_D/H_E = M_z(0)/M_0$, where $M_z(0)$ is the WFM component of the Fe-sublattice.

The hysteresis loops recorded at T = 5 K for $YFeO_3$ samples (Figure 10) show a linear decrease starting from the maximum magnetic field (70 kOe) and down to H = 0 kOe, due to the WFM component of the Fe sublattices. Because the canting angle between Fe sublattices is given by $\alpha = {}^1/_2 M_z(0)/M_0$, the WFM component can be directly estimated from extrapolation of M(H, 5 K) to H = 0 kOe, yielding $M_z(0) = 1.23(1)$ emu/g, similar to previous reports.[48] From this value one finds the net contribution of the iron sublattice to be $M_z(0) = 4.2 \times 10^{-2}\ \mu_B$, corresponding to a canting angle $\alpha \approx 8.5$ mrad for the Fe moments, assuming that the magnetic moment of the Fe^{3+} ions is $\mu_{eff} = 5\ \mu_B$. The α value is similar to previous values reported for $YFeO_3$ orthoferrite from Mössbauer and magnetization measurements.[40,41] Some minor differences were observed in the low-field region (H $\approx$ 20 kOe), for instance, the coercivity of the sample calcined at 1200 °C (**YF3**) showed the largest value, and the smallest jump at H = 0 kOe. As the large anisotropy is related to the rotation of the net sublattice moment out of the DM plane, it could be related to an enhancement of the exchange (i.e., DM) interactions for sample **YF3**.

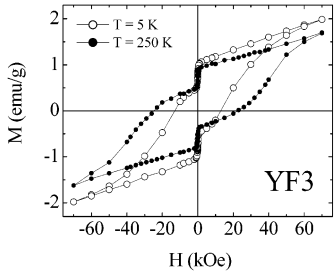

Figure 11. Hysteresis loops recorded for the sample **YF3** at 5 K (open circles) and 250 K (filled circles).

The M(H) curves showed a large increase of the coercive field with increasing temperatures, attaining a value of $H_C = 24.6(1)$ kOe at T = 250 K for sample **YF3**, as shown in Figure 11. Although the origin of this dependence is not yet clear, the large H_C value should arise from thermal dependence of H_D or H_E anisotropy fields. Previous works on the temperature dependence of the Hamiltonian of eq 4 have shown that, for a correct fitting of experimental M(T) and M(H) data, an additional cubic anisotropy term is needed in eq 4.[50,51]

Following Treves[42,49] we have calculated the exchange field H_E by using the relation $H_E = M_0/\chi$ and the previously assumed value $\mu_{eff}(Fe^{3+}) = 5\ \mu_B$ (i.e., M_0 = 72.5 emu/g), obtaining $H_E = 5.6 \times 10^6$ Oe. We have also estimated the DM anisotropy field by using the relation $H_D = M_z(0)/\chi$ and the value $\chi = 1.3 \times 10^{-5}$ emu·g^{-1}·Oe^{-1} (extracted from the linear region of the M(H) curves). The value $H_D = 9.5 \times 10^4$ Oe obtained in this way is close to that in previous reports on $YFeO_3$.[37,38] On comparing Figures 10 and 11, it can be observed that the difference of coercive fields between samples **YF1** and **YF3** is much less (~500 Oe) than the effect of temperature (~10 kOe between 5 and 250 K in sample **YF3**). The H_C values observed (~2.5×10^4 Oe) are smaller than the anisotropy field H_D related to the reversion of the WFM moment. However, the hysteresis cycle remains open to the largest field attained in this experiment (70 kOe), and so it does not correspond to a

(44) Hendriksen, P. V.; Linderoth, S.; Lindgard, P. A. *J. Phys.: Condens. Mater.* **1993**, *5*, 5675.
(45) Xiao, G.; Chien, C. L. *J. Appl. Phys.* **1987**, *61*, 3308.
(46) Martínez, B.; Roig, A.; Obradors, X.; Molins, E.; Rouanet, A.; Monty, C. *J. Appl. Phys.* **1996**, *79*, 2580.
(47) Jarjayes, O.; Fries, P. H.; Bidan, G. *J. Magn. Magn. Mater.* **1994**, *137*, 205.
(48) Goya, G. F.; Berquó, T. S.; Fonseca, F. C.; Morales, M. P. *J. Appl. Phys.* **2003**, *94*, 3520.
(49) Treves, D. *J. Appl. Phys.* **1965**, *36*, 1033.
(50) Gorodetsky, G.; Shtrikman, S.; Tenembaum, Y.; Treves, D. *Phys. Rev.* **1969**, *181*, 823.
(51) Wolf, W. P. *Phys. Rev.* **1957**, *108*, 1152.

major loop. Therefore, our samples should display even higher coercivities after being magnetized in higher fields.

We note also that the above interpretation of M(H) curves in orthoferrites differs from the two-phase model proposed by Schmool et al. for $YFeO_3$, where a small (residual) coercivity was attributed to a magnetically soft secondary ($Y_3Fe_5O_{12}$) phase.[17,35] The present data show that the peculiar shape is an intrinsic property of $(RE)FeO_3$ phases, explainable by the WFM character of these systems.

Conclusions

Inorganic materials prepared from molecular precursors represent an important facet of the Molecules-to-Materials approach. Molecular routes allow a kinetic control over the phase evolution and provide a means to prepare materials that are thermodynamically less favored (metastable). This work demonstrates the synthesis of nanoscopic yttrium orthoferrite as a single phase material by the sol−gel processing of precursor $[YFe(OPr^i)_6(Pr^iOH)]_2$. Orthoferrites are difficult to prepare as pure materials because of the facile and preferred formation of the garnet composition in Y_2O_3−Fe_2O_3 system. In contrast to the difficulties associated with the conventional processing methods, the use of a single molecular precursor is effective in producing monophasic $YFeO_3$. Further, crystalline samples with a narrow size-distribution were obtained at remarkably reduced crystallization temperature (680 °C) when compared to that of solid-state synthesis (>1000 °C). More importantly, the samples were compositionally pure and no element segregation or crystallization of other stoichiometries was observed even at high calcination temperature (>1300 °C). The relatively large values of magnetocrystalline anisotropy indicates a high local atomic ordering in the samples that would facilitate the Fe−O−Fe superexchange interactions. The hyperfine parameters in the Mössbauer spectra indicate well-crystallized samples, which was supported by TEM and XRD data. The magnetization measurements revealed low- and high-field regimes, corresponding to magnetocrystalline and antisymmetric-exchange anisotropy, respectively.

Acknowledgment. This work was supported in part by the Volkswagen Foundation, Germany. S.M. and M.V. are thankful to the German Science Foundation for providing financial support in the priority program SFB-277 on Nanocrystalline Materials. T.S.B., W.L.M.F., and G.F.G. are thankful to the Brazilian agencies FAPESP and CNPq for providing partial financial assistance.

CM0311729